Water Oxidation

DOI: 10.1002/anie.201407179

Photocatalytic Water Oxidation by a Pyrochlore Oxide upon Irradiation with Visible Light: Rhodium Substitution Into Yttrium Titanate**

*Borbala Kiss, Christophe Didier, Timothy Johnson, Troy D. Manning, Matthew S. Dyer, Alexander J. Cowan, John B. Claridge, James R. Darwent, and Matthew J. Rosseinsky**

Abstract: *A stable visible-light-driven photocatalyst ($\lambda \geq$ 450 nm) for water oxidation is reported. Rhodium substitution into the pyrochlore $Y_2Ti_2O_7$ is demonstrated by monitoring Vegard's law evolution of the unit-cell parameters with changing rhodium content, to a maximum content of 3% dopant. Substitution renders the solid solutions visible-light active. The overall rate of oxygen evolution is comparable to WO_3 but with superior light-harvesting and surface-area-normalized turnover rates, making $Y_2Ti_{1.94}Rh_{0.06}O_7$ an excellent candidate for use in a Z-scheme water-splitting system.*

The photocatalytic splitting of water by visible light using semiconductor materials has been proposed as a route to sustainable hydrogen generation.[1] Of the systems available, Z-scheme photocatalysis offers several advantages over single-particle photocatalysis or photoelectrocatalysis.[2] The Z-scheme system is inspired by natural photosynthesis in which two separate photocatalysts are linked by a shuttle redox mediator. In an artificial Z-scheme, each of the water splitting half-reactions is performed separately on each of the catalysts. Z-Scheme systems lower the energy required for photocatalysis as the valence and conduction band edges of the individual photocatalysts do not have to straddle the reduction potentials of H^+/H_2 and O_2/H_2O redox couples as they do for a single-particle photocatalyst. In this way a wider range of wavelengths of visible light can be used. Importantly, using the Z-scheme approach, water splitting can take place in a simple reactor without the requirement for potentially costly electrode connections and transparent conducting supports. The production of oxygen is a critical step in solar fuel production and is a requirement for any photocatalytic water-splitting system. This half of the water-splitting process is more challenging as it typically involves a four-electron process and powerful oxidizing species which can lead to breakdown of the photocatalyst. It is also essential for photoelectrolysis. Although significant effort has been expended on developing visible-light-active hydrogen-generating photocatalysts,[3] only a very limited number of stable, visible-light-active oxygen-evolving photocatalysts are known.[4] Monoclinic WO_3 has been extensively studied as an oxygen-generating photocatalyst and is generally used as the standard comparative material because of its commercial availability and reasonable performance.[5] However WO_3 has a relatively large band gap (2.6 eV) limiting its absorption of visible light to $\lambda < 480$ nm. Nanostructured $BiVO_4$ ($E_g \approx$ 2.4 eV)[6] has been shown to photocatalytically generate oxygen under irradiation with visible light and has a similar activity to WO_3.[7] Oxynitride perovskites have also displayed photocatalytic oxygen generation[8] but are less stable to photocorrosion than oxide materials unless OH^- is removed in situ by the addition of La_2O_3.[9] Recently, Ag_3PO_4 has been demonstrated as a highly efficient oxygen-evolving photocatalyst[10] though questions remain over its stability under reaction conditions.[11] Therefore, to enable the development of an efficient Z-scheme photocatalytic system for water splitting, new stable, efficient, visible-light-active oxygen-evolving photocatalysts are urgently required as highlighted in the recent review by Ma and co-workers.[12]

The first reported photocatalyst for water splitting under irradiation with ultraviolet (UV) light was TiO_2.[13] As a consequence, considerable attention has been given to titanium oxides including the perovskite $SrTiO_3$ which also has photocatalytic activity for water splitting under irradiation with UV light.[14] Several alternatives for Ti-based materials have been evaluated to render these materials active under visible light[15] with Rh reported as one of the most effective;[15b] $SrTi_{1-x}Rh_xO_3$ with a Pt-containing co-catalyst in an aqueous CH_3OH solution is a highly-active hydrogen-evolving photocatalyst under visible light and has been used with $BiVO_4$ or with WO_3 in a Z-scheme photocatalytic system to split water with visible light.[16] Calculations[17] suggest that rhodium E_g states are located within the conduction band in $SrTi_{1-x}Rh_xO_3$, allowing visible-light excitation from the rhodium-based T_{2g} state to generate delocalized electrons which evolve hydrogen. However, the formation of Rh^{4+} inter-gap states, which act as a recombina-

[*] B. Kiss, Dr. C. Didier, T. Johnson, Dr. T. D. Manning, Dr. M. S. Dyer, Dr. J. B. Claridge, Prof. J. R. Darwent, Prof. M. J. Rosseinsky
Department of Chemistry
University of Liverpool
Liverpool, L69 7ZD (UK)
E-mail: M.J.Rosseinsky@liverpool.ac.uk
Dr. A. J. Cowan
Stephenson Institute for Renewable Energy
University of Liverpool, Liverpool, L69 7ZF (UK)

[**] This work is funded by EPSRC (EP/H000925). A.J.C. acknowledges the EPSRC for Fellowship EP/K006851/1. Computational resources were provided on ARCHER, through the UK's HPC Materials Chemistry Consortium, and funded by the EPSRC (EP/L000202). Dr. R. Treharne is thanked for constructive conversations on the fitting of optical data.

Supporting information for this article is available on the WWW under http://dx.doi.org/10.1002/anie.201407179.

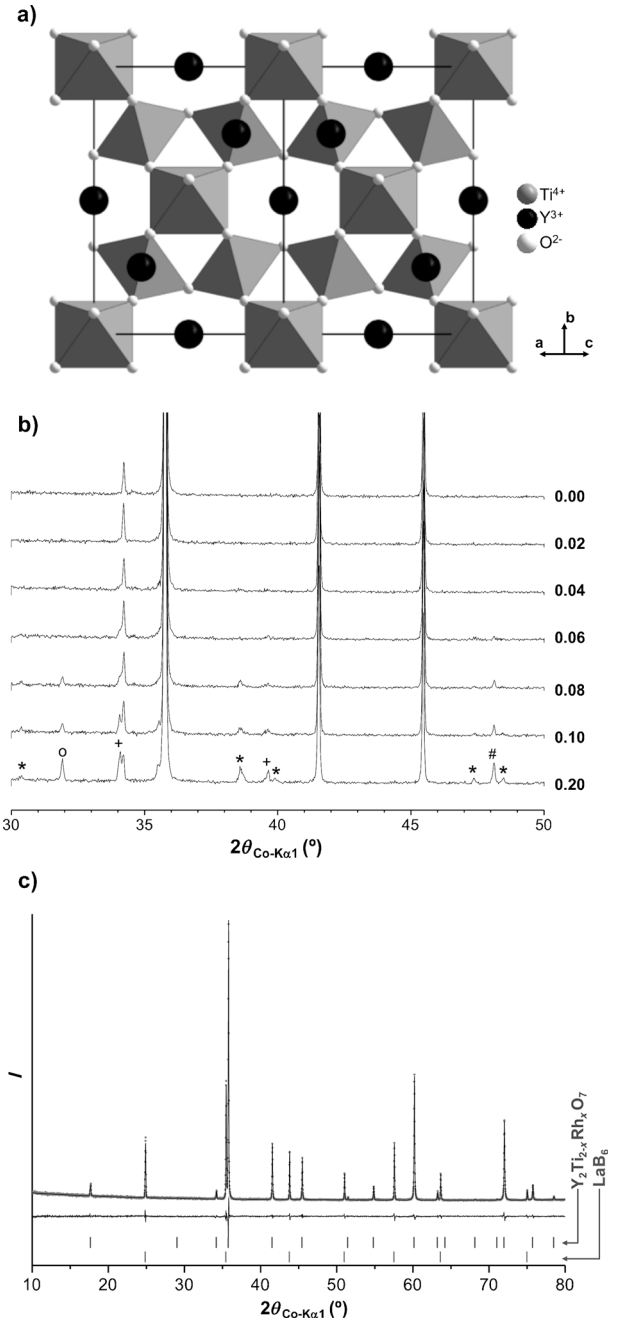

Figure 1. a) Unit cell of the pyrochlore structure projected along the [101] direction. Six-coordinate Ti^{4+} sites are represented by a network of gray corner-sharing octahedra. Y^{3+} and O^{2-} ions are represented by black and white spheres. b) Enlargement of the powder XRD patterns of $Y_2Ti_{2-x}Rh_xO_7$ with $0 \le x \le 0.2$ at the base of the peaks, showing impurities for $x > 0.06$. The main peaks ($x \ge 0$) denote the phase-pure cubic pyrochlore. Impurities are indicated on the $x = 0.2$ doped sample: # Rh; o TiO_2; + Y_2O_3; * $YRhO_3$. c) Le Bail whole-pattern fitting of $Y_2Ti_{1.98}Rh_{0.02}O_7$, with LaB_6 as an internal standard.

tion center for photoexcited carriers, can inhibit hydrogen evolution.

The $A_2B_2O_7$ pyrochlore structure (Figure 1a) consists of corner-sharing BO_6 octahedra with A cations in a 2 + 6 environment, with is one B-O-B angle which is approximately 135°.[18] The rare-earth $R_2Ti_2O_7$ pyrochlores thus have some structural similarities with perovskite $SrTiO_3$, which also features a corner-sharing TiO_6 octahedral network but with angles much closer to 180°. Pyrochlore is an important type of ternary oxide which sustains a range of functions and is extensively tunable by substitution.[18] Abe et al. have shown that pyrochlore $Y_2Ti_2O_7$ with a NiO_x co-catalyst can be successfully used as a photocatalyst for water splitting under irradiation with UV light, with a band gap of 3.5 eV.[19] As this gap is much larger than that of $SrTiO_3$ (3.2 eV), the Rh-derived E_g states in $Y_2Ti_{2-x}Rh_xO_7$ may sit just below the conduction band edge and thus become localized, potentially acting as recombination states or becoming photocatalytically inactive to hydrogen generation. The extensive chemical tunability of pyrochlore suggests that suitable substitutions would enhance its photocatalytic properties and open up new directions in the synthesis of photocatalysts. Herein, we report the phase-pure pyrochlore $Y_2Ti_{2-x}Rh_xO_7$ solid solution series and demonstrates its stable visible-light activity as an oxygen-evolving photocatalyst. Experiments using this material in suspension establish it as a promising candidate for inclusion in a Z-scheme photocatalytic system but we also note that $Y_2Ti_{2-x}Rh_xO_7$ is a potential photoanode.

The powder X-ray diffraction (XRD) patterns of the $Y_2Ti_{2-x}Rh_xO_7$ samples, prepared by solid-state synthesis and with $0 \le x \le 0.2$, are shown in Figure 1b and in Figure S1 in the Supporting Information. All the samples contain a pyrochlore phase. However, as the comparison between Figure S1 and Figure 1b emphasizes, it is easy to miss crystalline impurities without a finer examination of the pattern. Non-pyrochlore peaks are detected for doping levels higher than $x = 0.06$, and have been assigned to Rh metal,[20] rutile TiO_2,[21] Y_2O_3,[22] and perovskite $YRhO_3$.[23] The presence of metallic rhodium results from conversion of Rh_2O_3 into the metal at temperatures above 1100 °C.[24] This suggests that $x = 0.06$ is the maximum amount of rhodium that can be inserted into the pyrochlore $Y_2Ti_2O_7$, however the presence of impurities that are not visible from XRD cannot be excluded. A better proof of Rh substitution into the pyrochlore structure is the evolution of the unit-cell dimensions upon substitution (Vegard's law).[25]

An internal standard was thus added to permit precise and accurate lattice-parameter determination. The unit-cell parameters of the pyrochlore $Y_2Ti_{2-x}Rh_xO_7$ were derived from whole-pattern fitting using the Le Bail method.[26] An example of the refinement profile is given in Figure 1c. The derived evolution of the cubic unit-cell parameter with increasing Rh concentration (Figure 2) is linear to $x = 0.08$, after which the unit-cell parameter is constant. This behavior confirms the insertion of rhodium into the pyrochlore structure at these concentrations. Since the $x = 0.08$ sample was not phase pure, $x = 0.06$ is the maximum amount of Rh that can be substituted into $Y_2Ti_2O_7$ under the synthetic conditions used herein. The ionic radii of the Rh^{4+} ion (0.615 Å[27] or 0.60 Å,[28] though 0.6 Å is based on values from a number of metallic oxides) and Ti^{4+} (0.605 Å)[28] are very close, whereas that of the Rh^{3+} center (0.665 Å)[28] is significantly larger. The unit-cell-parameter changes measured are expected to be comparatively small in any solid solution based on isovalent substitution, consistent with

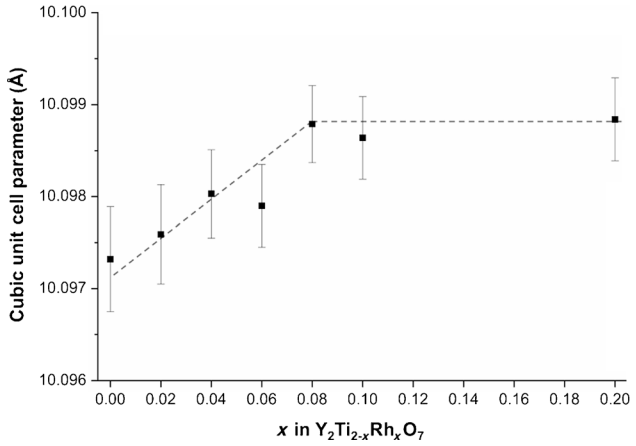

Figure 2. Unit cell parameter of $Y_2Ti_{2-x}Rh_xO_7$ determined from whole-pattern fitting using the Le Bail method with LaB_6 employed as the internal standard. Error bars are 3×e.s.d. (estimated standard deviation) obtained from the refinement procedure, with Berar's factor included to ensure correlations are accounted for appropriately.

rhodium being present as Rh^{4+}. Substitution of Rh centers for Y is unlikely as the size difference between these cations is significant (1.019 Å for Y^{3+}),[28] and eightfold or higher coordination for rhodium ions is very unusual. This substitution would also generate excess Y_2O_3 in the phase assemblage, which is not detected below the solubility limit (Figure 1). The possibility of substitution of Rh centers for Y in the $Y_2Ti_2O_7$ pyrochlore can thus be safely excluded.

The UV/Vis absorption spectra, derived from the conversion of the diffuse reflection spectra, of $Y_2Ti_{2-x}Rh_xO_7$ ($0 \le x \le 0.06$) are shown in Figure 3a. The parent $Y_2Ti_2O_7$ material has a measured indirect band gap of 3.71 eV (Figure S8) and does not absorb visible light.[19,29] Substitution of Rh into $Y_2Ti_2O_7$ produces significant changes in the spectral response, with a red shift of the absorption edge, together with the presence of two entirely new absorption bands in the visible region of the spectrum, giving light absorption down to $\lambda = 700$ nm (Figure 3a, Figure S9).

Visible-light absorption bands in rhodium(IV)-substituted $SrTiO_3$ are associated with d–d transitions between Rh states just above the valence band and to a Rh inter-gap state and the conduction band.[15b,17,30] DFT calculations of the density of states (DOS) of $Y_2Ti_{1.75}Rh_{0.25}O_7$ (Figure 3b) reveal that, in addition to the inter-gap and near-valence-band states, rhodium-based d states are also evident just below the conduction band of $Y_2Ti_2O_7$ upon Rh substitution. The computed DOS suggests that the lowest energy absorption band ($\lambda = 560$ nm) results from a d–d transition from Rh d states just above the valence band to the inter-gap state, and that the feature at $\lambda = 420$ nm is a transition from the valence band edge to the inter-gap state. The shift in the absorption band edge to lower energy cannot be attributed to a change in the fundamental O(2p)–Ti(3d) band gap, which remains almost unchanged in calculations. Instead, a combination of transitions involving the localized rhodium-based d states just above the valence band and those just below the conduction band have energies lower than the fundamental band gap, and

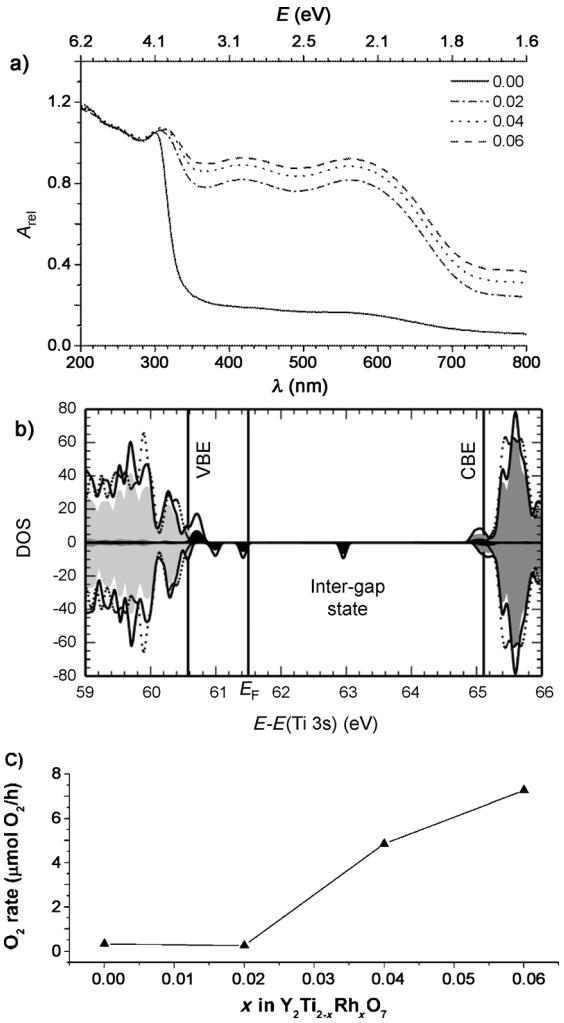

Figure 3. a) UV/Vis absorption spectra derived from diffuse reflection spectra of $Y_2Ti_{2-x}Rh_xO_7$ ($0 \le x \le 0.06$). b) The DOS of $Y_2Ti_2O_7$ (dotted line) and $Y_2Ti_{1.875}Rh_{0.125}O_7$ (solid line) are plotted along with the partial DOS projected onto the Ti 3d (mid-gray shaded), Rh 4d (black shaded) and O 2p (light-gray shaded) orbitals of $Y_2Ti_{1.875}Rh_{0.125}O_7$ using the energy of the Ti 3s states as a common reference energy. The computed valence band edge (VBE) and conduction band edge (CBE) of $Y_2Ti_2O_7$ are indicated as vertical lines, along with the calculated Fermi energy (E_F) of $Y_2Ti_{1.875}Rh_{0.125}O_7$. c) Rate of O_2 generation using $Y_2Ti_{2-x}Rh_xO_7$ under visible light. Conditions: catalyst (0.1 g); no co-catalyst; 20 mL of a $AgNO_3$ solution (aq; 0.05 M); 300 W Xe lamp ($\lambda > 420$ nm; $\lambda < 2.95$ eV).

effectively reduce the energy of the adsorption edge. On this basis the spectra have been fitted to two Gaussian peaks, an exponential function for the Urbach tail and a power-law-dependent absorption edge (see Section 8 in the Supporting Information for details), with a red shift of the absorption band edge to 3.12 eV for $x = 0.06$ and a tail that extends into the visible region of the spectrum. The visible-light activity of $Y_2Ti_{2-x}Rh_xO_7$ is as a result of one or more of the transitions arising from the incorporation of Rh into the material and leads to absorption bands in the visible region of the electromagnetic spectrum.

The $Y_2Ti_{2-x}Rh_xO_7$ series were investigated as photocatalysts for the evolution of H_2 and O_2 from water with visible

light. No H_2 evolution was detected under illumination with visible light using a 300 W Xenon lamp with a $\lambda = 420$ nm cut-off filter for any material, in the presence or the absence of a co-catalyst. The materials did however display visible-light activity for O_2 generation.

The O_2 evolution rate, measured with a Clark electrode,[5,31] for unloaded $Y_2Ti_{2-x}Rh_xO_7$ ($0 \le x \le 0.06$) is represented in Figure 3c. Materials in which $x = 0$ and $x = 0.02$ did not show visible-light activity. However, visible-light photocatalytic O_2 evolution is detected for samples with $x \ge 0.04$. The activity increases up to $x > 0.06$ where it reaches a plateau, and $Y_2Ti_{1.94}Rh_{0.06}O_7$ displays excellent recyclability with no significant change in oxygen evolution rate over three cycles (Figure 4). The samples were examined by scanning electron microscopy (SEM) and powder XRD (Figure S2 and S3) before and after the photocatalytic measurements and no indication of photocorrosion was detected. Oxygen evolution rates for both WO_3, studied as a benchmark, and $Y_2Ti_{1.94}Rh_{0.06}O_7$ were confirmed by the widely used GC method using the same solution conditions as for the Clark electrode experiments and $\lambda = 400 \pm 5$ nm irradiation (Figure S4). Turnover rates per unit mass (TOR_m) and per unit surface area (TOR_s) have been suggested as useful comparisons between photocatalytic materials.[32] TOR_m for $Y_2Ti_{1.94}Rh_{0.06}O_7$ and WO_3 are similar (73 and 71 $\mu mol\,g^{-1}\,h^{-1}$ respectively, Table S4). However there was a significant difference in TOR_s values. The commercial WO_3 nanopowder has a Brunauer—Emmett—Teller (BET) surface area of 9.1 $m^2\,g^{-1}$ giving $TOR_s = 7.9\ \mu mol\,m^{-2}\,h^{-1}$; $Y_2Ti_{1.94}Rh_{0.06}O_7$ has a surface area of 3.2 $m^2\,g^{-1}$ giving $TOR_s = 22.8\ \mu mol\,m^{-2}\,h^{-1}$ (Table S4). This suggests that increasing the surface area of $Y_2Ti_{1.94}Rh_{0.06}O_7$ by using alternative synthetic methods may further increase the photocatalytic activity of the material. For example sol–gel synthetic routes for $Y_2Ti_2O_7$ have been reported by several groups.[33] Apparent quantum-efficiency values are given in Table S3: $Y_2Ti_{1.94}Rh_{0.06}O_7$ is superior to WO_3 at $\lambda = 450$ nm and comparable at $\lambda = 400$ nm under the illumination conditions used.

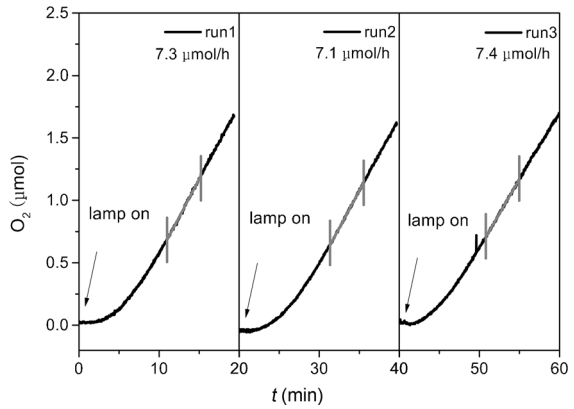

Figure 4. Recyclability of $Y_2Ti_{1.94}Rh_{0.06}O_7$ oxygen-evolution photocatalyst. Conditions: catalyst (0.1 g); no co-catalyst; 20 mL of a $AgNO_3$ solution (aq; 0.05 M); 300 W Xe lamp light source with a $\lambda > 420$ nm cut-off filter. The gray lines mark where the O_2 reaction rate was measured ($\mu mol\,min^{-1}$).

The addition of co-catalysts for water oxidation is a widely employed approach to enhance photocatalytic activity. As well as for the pure catalysts, the effect of five of the most widely studied co-catalysts (Pt^0, Ru^0, Ni^0, RuO_2, $Rh_{2-y}Cr_yO_3$), identified to enhance the photocatalytic activity of other oxides for hydrogen and/or oxygen evolution, was investigated.[8] Procedures for co-catalyst loadings are provided in the Supporting Information. Only the 1% RuO_2-loaded $Y_2Ti_{1.94}Rh_{0.06}O_7$ showed a slight enhancement of the evolution rate (7.6 $\mu mol\,h^{-1}$) (Table S1, Figure S10 and S11). Similarly, an enhanced O_2 evolution rate was reported for RuO_2/WO_3.[31a] Interestingly, Ru metal loading (Figure S11) resulted in a large drop of the O_2 evolution activity. This inhibiting mechanism of the Ru^0 center in O_2 evolution has also been reported for Ru^0/WO_3.[31a] It is in fact not uncommon for a co-catalyst to reduce the activity of O_2 evolution.[34,35] Decreased photocatalytic activity in the presence of a co-catalyst is typically proposed to be because of increased electron–hole recombination losses, with either the co-catalysts themselves acting as recombination centers[34] or the deposition process leading to surface modifications and the formation of undefined recombination sites.

Advances in semiconductor materials for light-driven proton reduction to H_2 and for CO_2 reduction to carbon-based fuels, such as CH_3OH, have led to an urgent requirement for improved, stable, visible-light-active water oxidation photocatalysts. Herein, we demonstrate that $Y_2Ti_{2-x}Rh_xO_7$ ($0.04 \le x \le 0.06$) is an efficient visible light photocatalyst for the generation of oxygen from water without the need for a co-catalyst. This opens potential for the pyrochlore structure class for wider use as photoelectrodes and in Z-scheme photocatalytic systems for the production of solar fuels.

Received: July 14, 2014
Revised: September 1, 2014
Published online: December 2, 2014

Keywords: photocatalysis · pyrochlore · rhodium · titanates · water splitting

[1] a) *The Hydrogen Economy: Opportunities, Costs, Barriers, and R&D Needs*, The National Academies Press, Washington D.C., **2004**; b) *Report of the Basic Energy Sciences Workshop on Hydrogen Production, Storage and Use*, Argonne National Laboratory, **2004**.
[2] K. Maeda, *ACS Catal.* **2013**, *3*, 1486 – 1503.
[3] F. Fresno, R. Portela, S. Suarez, J. M. Coronado, *J. Mater. Chem. A* **2014**, *2*, 2863 – 2884.
[4] L. Yang, H. Zhou, T. Fan, D. Zhang, *Phys. Chem. Chem. Phys.* **2014**, *16*, 6810 – 6826.
[5] W. Erbs, J. Desilvestro, E. Borgarello, M. Grätzel, *J. Phys. Chem.* **1984**, *88*, 4001 – 4006.
[6] A. Walsh, Y. Yan, M. N. Huda, M. M. Al-Jassim, S.-H. Wei, *Chem. Mater.* **2009**, *21*, 547 – 551.
[7] A. Kudo, K. Omori, H. Kato, *J. Am. Chem. Soc.* **1999**, *121*, 11459 – 11467.
[8] T. Hisatomi, J. Kubota, K. Domen, *Chem. Soc. Rev.* **2014**, *43*, 7520 – 7535.

[9] T. Takata, G. Hitoki, J. N. Kondo, M. Hara, H. Kobayashi, K. Domen, *Res. Chem. Intermed.* **2007**, *33*, 13 – 25.
[10] a) Z. Yi, J. Ye, N. Kikugawa, T. Kako, S. Ouyang, H. Stuart-Williams, H. Yang, J. Cao, W. Luo, Z. Li, Y. Liu, R. L. Withers, *Nat. Mater.* **2010**, *9*, 559 – 564; b) D. J. Martin, N. Umezawa, X. Chen, J. Ye, J. Tang, *Energy Environ. Sci.* **2013**, *6*, 3380 – 3386.
[11] Y. Bi, S. Ouyang, J. Cao, J. Ye, *Phys. Chem. Chem. Phys.* **2011**, *13*, 10071 – 10075.
[12] Y. Ma, X. Wang, Y. Jia, X. Chen, H. Han, C. Li, *Chem. Rev.* **2014**, *114*, 9987 – 10043.
[13] A. Fujishima, K. Honda, *Nature* **1972**, *238*, 37 – 38.
[14] K. Domen, S. Naito, M. Soma, T. Onishi, K. Tamaru, *J. Chem. Soc. Chem. Commun.* **1980**, 543 – 544.
[15] a) H. Kato, A. Kudo, *J. Phys. Chem. B* **2002**, *106*, 5029 – 5034; b) R. Konta, T. Ishii, H. Kato, A. Kudo, *J. Phys. Chem. B* **2004**, *108*, 8992 – 8995; c) R. Niishiro, H. Kato, A. Kudo, *Phys. Chem. Chem. Phys.* **2005**, *7*, 2241 – 2245; d) R. Asahi, T. Morikawa, T. Ohwaki, K. Aoki, Y. Taga, *Science* **2001**, *293*, 269 – 271.
[16] Y. Sasaki, H. Nemoto, K. Saito, A. Kudo, *J. Phys. Chem. C* **2009**, *113*, 17536 – 17542.
[17] S. Kawasaki, K. Akagi, K. Nakatsuji, S. Yamamoto, I. Matsuda, Y. Harada, J. Yoshinobu, F. Komori, R. Takahashi, M. Lippmaa, C. Sakai, H. Niwa, M. Oshima, K. Iwashina, A. Kudo, *J. Phys. Chem. C* **2012**, *116*, 24445 – 24448.
[18] M. A. Subramanian, G. Aravamudan, G. V. Subba Rao, *Prog. Solid State Chem.* **1983**, *15*, 55 – 143.
[19] R. Abe, M. Higashi, K. Sayama, Y. Abe, H. Sugihara, *J. Phys. Chem. B* **2006**, *110*, 2219 – 2226.
[20] H. E. Swanson, R. K. Fuyat, *Natl. Bur. Stand.* **1953**, *circ. 539*, *vol. 2*.
[21] F. Schoβberger, *Z. Kristallogr. Kristallgeom. Kristallphys. Krista* **1942**, *104*, 358 – 374.
[22] Ľ. Smrčok, P. Ďuriš in *X-Ray and Neutron Structure Analysis in Materials Science* (Ed.: J. Hašek), Springer, New York, **1989**, pp. 375 – 378.
[23] V. B. Lazarev, I. S. Shaplygin, *Russ. J. Inorg. Chem.* **1978**, *23*, 2614 – 2621.
[24] *CRC Handbook of Chemistry and Physics*, 80th ed., CRC, Boca Raton, **1999 – 2000**.
[25] A. R. West, *Solid State Chemistry and its Applications*, 2nd ed., Wiley, Hoboken, **2013**.
[26] A. Le Bail, H. Duroy, J. L. Fourquet, *Mater. Res. Bull.* **1988**, *23*, 447 – 452.
[27] R. D. Shannon, C. T. Prewitt, *Acta Crystallogr. Sect. B* **1969**, *25*, 925 – 946.
[28] R. Shannon, *Acta Crystallogr. Sect. A* **1976**, *32*, 751 – 767.
[29] B. V. Kumar, R. Velchuri, V. R. Devi, G. Prasad, B. Sreedhar, C. Bansal, M. Vithal, *J. Appl. Phys.* **2010**, *108*, 044906.
[30] R. Niishiro, R. Konta, H. Kato, W.-J. Chun, K. Asakura, A. Kudo, *J. Phys. Chem. C* **2007**, *111*, 17420 – 17426.
[31] a) J. R. Darwent, A. Mills, *J. Chem. Soc. Faraday Trans. 2* **1982**, *78*, 359 – 367; b) Y. Zhang, J. Rosen, G. S. Hutchings, F. Jiao, *Catal. Today* **2014**, *225*, 171 – 176; c) N. M. Dimitrijevic, S. Li, M. Grätzel, *J. Am. Chem. Soc.* **1984**, *106*, 6565 – 6569.
[32] I. E. Wachs, S. P. Phivilay, C. A. Roberts, *ACS Catal.* **2013**, *3*, 2606 – 2611.
[33] a) O. Merka, D. W. Bahnemann, M. Wark, *ChemCatChem* **2012**, *4*, 1819 – 1827; b) O. Merka, O. Raisch, F. Steinbach, D. W. Bahnemann, M. Wark, *J. Am. Ceram. Soc.* **2013**, *96*, 634 – 642; c) M. Higashi, R. Abe, K. Sayama, H. Sugihara, Y. Abe, *Chem. Lett.* **2005**, *34*, 1122 – 1123.
[34] T. Sakata, K. Hashimoto, T. Kawai, *J. Phys. Chem.* **1984**, *88*, 5214 – 5221.
[35] J. Yang, D. Wang, H. Han, C. Li, *Acc. Chem. Res.* **2013**, *46*, 1900 – 1909.

